Velocity dispersion at Long Beach

Jason P. Chang

ABSTRACT

Previous studies from the dense Long Beach, California, seismic array have shown that both surface waves and P-waves can be recovered by seismic interferometry. In this report, I focus on constraining the apparent velocities of the wave types by performing τ-p transforms and generating dispersion images. From τ-p transforms, I find that the velocity of P-waves is approximately 2500 m/s. My dispersion analysis reveals that I am recovering the fundamental Rayleigh wave mode, as well as the first-order mode. Both observed Rayleigh-wave modes are dispersive, with the waves travelling faster at lower frequencies than at higher frequencies. I also find that the first-order mode travels at a greater velocity than the fundamental mode over the range of frequencies that I investigated.

INTRODUCTION

Characterizing near-surface regions ($<$ 100 m depth) is of primary importance in a number of fields, including engineering seismology, where shear wave velocities are useful for earthquake hazard analysis, and hydrogeology, where the depth of the water table can be determined from seismic data. Traditional methods for collecting near-surface seismic information in urban environments are disruptive and difficult to perform. Seismic interferometry provides an alternative method, and the Long Beach, California, seismic array is particularly well-suited for urban seismic interferometry. Deployed by Nodal Seismic, Inc. in January 2012, the array is both dense, consisting of 2400 vertical-component geophones with an average spacing of 100 m (Figure 1), and of long duration, recording continuously (24 hrs/day) for over three months.

From this Long Beach dataset, Chang et al. (2013) showed that Rayleigh waves originating from the Pacific Ocean could be recovered between 0.5 and 2.0 Hz from a week of ambient seismic noise recordings. Furthermore, they showed that by stacking over multiple virtual sources, P-waves could be recovered between 2.0 and 4.0 Hz from nearly three weeks of ambient noise recordings. From this virtual super-source gather, they estimated the P-wave to be propagating at a velocity of approximately 2000 m/s.

The goal of this report is to better constrain the apparent velocity estimates from Chang et al. (2013) for both Rayleigh and P-waves. First, I generate virtual source gathers using seismic interferometry. I then perform τ-p transforms and generate

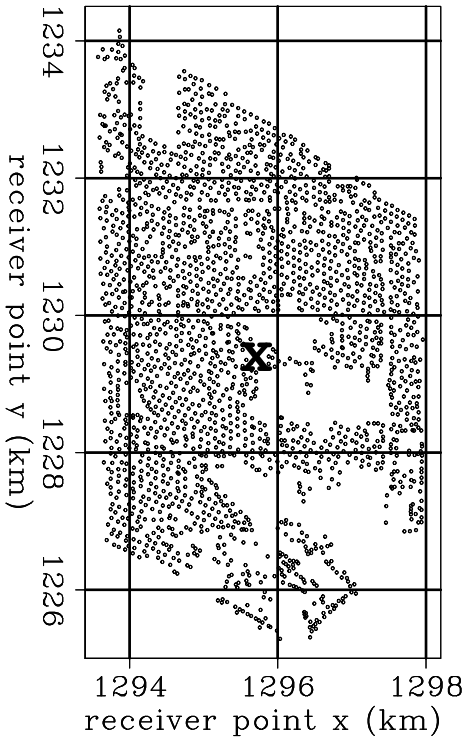

Figure 1: Map of the Long Beach array. 'X' marks the location of the virtual source. Coordinates are NAD27, CA State Plane, Zone 7, kilometers. [**ER**]

dispersion images from those virtual source gathers to better constrain the apparent velocities of the wave types.

VIRTUAL SOURCE GATHERS FROM LONG BEACH

Seismic interferometry states that the Green's function between two receivers can be obtained by cross-correlating records of ambient seismic noise from two simultaneously recording receivers over a long period of time (Wapenaar et al., 2010). In other words, I can generate virtual seismic sources using seismic interferometry. To generate my estimated Green's functions (EGFs), I follow the processing method adapted from Bensen et al. (2007). I first break up the time series into tapered, non-overlapping two-hour time windows. I then whiten the input traces and bandpass filter prior to cross-correlating. In the frequency domain, the cross-correlation of pre-whitened traces can be expressed as

$$[G(x_B, x_A, \omega) + G^*(x_B, x_A, \omega)] = \left\langle \left(\frac{U(x_B, \omega)}{\{|U(x_B, \omega)|\}} \right) \left(\frac{U^*(x_A, \omega)}{\{|U(x_A, \omega)|\}} \right) \right\rangle \quad , \qquad (1)$$

where G is the Green's function between two receiver locations (x_A, x_B), $U(x, \omega)$ is the spectrum of the wavefield at a given receiver location x, $*$ represents the complex conjugate, $\langle \cdot \rangle$ represents the time-averaged ensemble, $|\cdot|$ represents the real absolute value of the spectrum, and $\{\cdot\}$ represents a 0.003 Hz running window average used for whitening the signal. By dividing the standard cross-correlation procedure by

smoothed amplitude spectrums at the two receivers, I am deconvolving an estimate of the noise source signal from the correlations in the time domain to obtain a better EGF.

Examples of virtual source gathers obtained from seismic interferometry can be seen in Figures 2 and 3. In Figure 2, I show traces that are bandpassed for 0.5-2.0 Hz. The virtual source location is shown in Figure 1. I average the correlations from 100 two-hour time windows, resulting in an average over 8 days. I then sort the traces by radial offset into 50 m bins and stack. Due to the inhomogeneous noise source distribution at Long Beach (Chang et al., 2013), I choose to improve the quality of the correlations by averaging the positive and negative time lag signals. In other words, I take the symmetric part of the correlations.

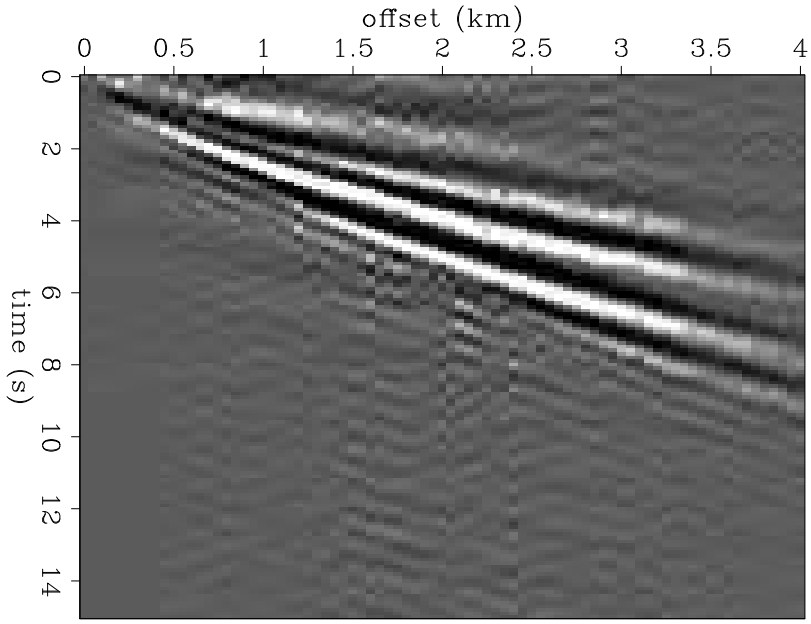

Figure 2: A virtual common source gather for frequencies between 0.5 Hz and 2.0 Hz. The virtual source location is labeled by 'X' in Figure 1. Traces have been sorted into 50 m radial offset bins. [**CR**]

In Figure 3, I display a virtual super-source gather for frequencies between 2 and 4 Hz. This is made by creating virtual source gathers from 100 randomly distributed source locations for each of the 240 two-hour time windows. This amounts to nearly 3 weeks of data and over 50 million correlations. I then sort all correlations by radial offset into 50 and 200 m bins, stack, and then symmetrize across zero time lag. Chang et al. (2013) used 200 m bins (Figure 3(a)) because it clearly revealed a P-wave that they estimated to be travelling at 2000 m/s based on the slope of the stepout. Here, I show that the P-wave is still visible with 50 m binning (Figure 3(b)), and that the surface waves are better resolved with finer binning. Hence, I will use the super-source gather with 50 m binning for further analysis.

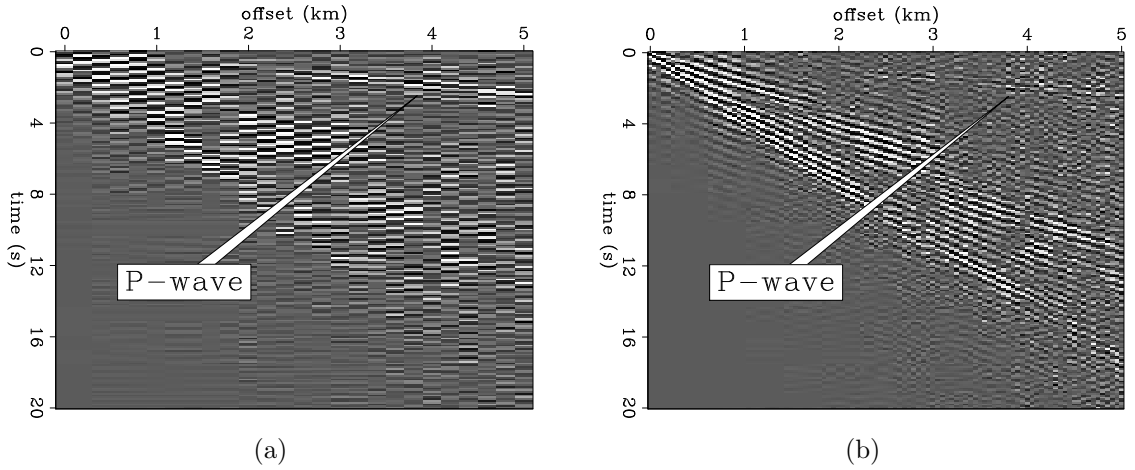

(a) (b)

Figure 3: Virtual super-source gathers for frequencies between 2 and 4 Hz. Left: 200 m offset binning. Right: 50 m offset binning. [**CR**]

τ-P TRANSFORMS

A τ-p transform, or slant stack, maps the gathers from the radial offset-time domain to the horizontal slowness-intercept time domain, or the τ-p domain. The transform is represented as

$$u'(p,\tau) = \int u(x, \tau + px)dx, \tag{2}$$

where u is the wavefield, u' is the transformed wavefield, x is radial offset, p is slowness or ray parameter (dt/dx), and τ is the time intercept or zero-offset reflection time (Claerbout, 1985; Stoffa, 1989). The transform extracts slowness information, as any coherent energy travelling at a certain slowness will stack constructively and appear as a strong event in the τ-p domain.

Figure 4(a) shows the gather in the τ-p domain for the lower frequency range (0.5-2.0 Hz). The anomaly appears quite spread out, meaning the Rayleigh waves do not travel at just one phase velocity. The slownesses are primarily bounded between 0.5 and 2.0 ms/m, or between 500 and 2000 m/s. Figure 4(b) shows the super-source gather in the τ-p domain for the higher frequency range (2-4 Hz). Again, there is a large anomaly that is representative of the Rayleigh waves. Here, the slownesses are primarily bounded between 1.4 and 2.7 ms/m, or between 370 and 710 m/s. It makes sense that Rayleigh-wave phase velocities are greater for lower frequencies than for higher frequencies, as lower frequencies typically sense deeper (and hence sense greater velocities) than higher frequencies.

There is also a smaller anomaly in Figure 4(b) near zero intercept time with a slowness of 0.4 ms/m, or 2500 m/s. This event is representative of the P-wave arrival. Whereas Chang et al. (2013) estimated the velocity of this arrival to be approximately 2000 m/s based on measuring the slope of the moveout with 200 m offset binning, the τ-p transform reveals that the apparent velocity is faster. This transform also shows

that although the P-wave is best revealed when radial offset is sorted into 200 m bins, the velocity is better measured with increasingly smaller bins.

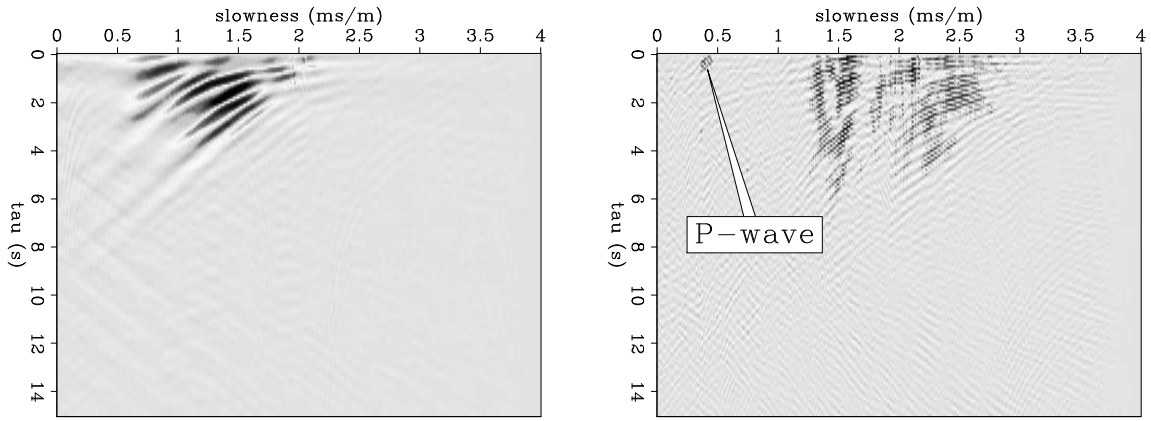

(a) (b)

Figure 4: τ-p transforms of the virtual source gathers with 50 m binning. Left: using the virtual source gather in Figure 2 for frequencies between 0.5 and 2.0 Hz. Right: using the virtual super-source gather in Figure 3(b) for frequencies between 2 and 4 Hz. [**CR**]

With a P-wave velocity of 2500 m/s, it is unlikely that this event is a refraction off the water table. However, more correlations will need to be stacked in to improve the quality of the gather at short offsets so that I can determine whether this P-wave is a critically refracted arrival or a direct arrival.

DISPERSION ANALYSIS

From the τ-p transformed gathers, it is clear that Rayleigh waves covered a range of velocities that varied with frequency content. To better see this behavior, I create dispersion images in the frequency-slowness domain. This is done by taking a one-dimensional Fourier transform along the intercept time axis of the τ-p transform. The resulting spectral peaks in the dispersion images indicate the phase slowness(es) associated with each frequency.

Figure 5(a) shows the dispersion image for a virtual source gather for the lower frequency range. There are two dispersive wave modes: the fundamental and the first-order Rayleigh wave modes. The stronger fundamental mode travels slower than the weaker first-order mode for a given frequency. For instance, at 0.8 Hz, there is a spectral peak centered near 1.5 ms/m, which corresponds to the fundamental mode travelling at 660 m/s, and a minor spectral peak near 0.9 ms/m, which corresponds to the first-order mode travelling at 1100 m/s.

Figure 5(b) shows the dispersion image for the virtual super-source gather for the higher frequency range. I examine the super-source gather rather than a normal

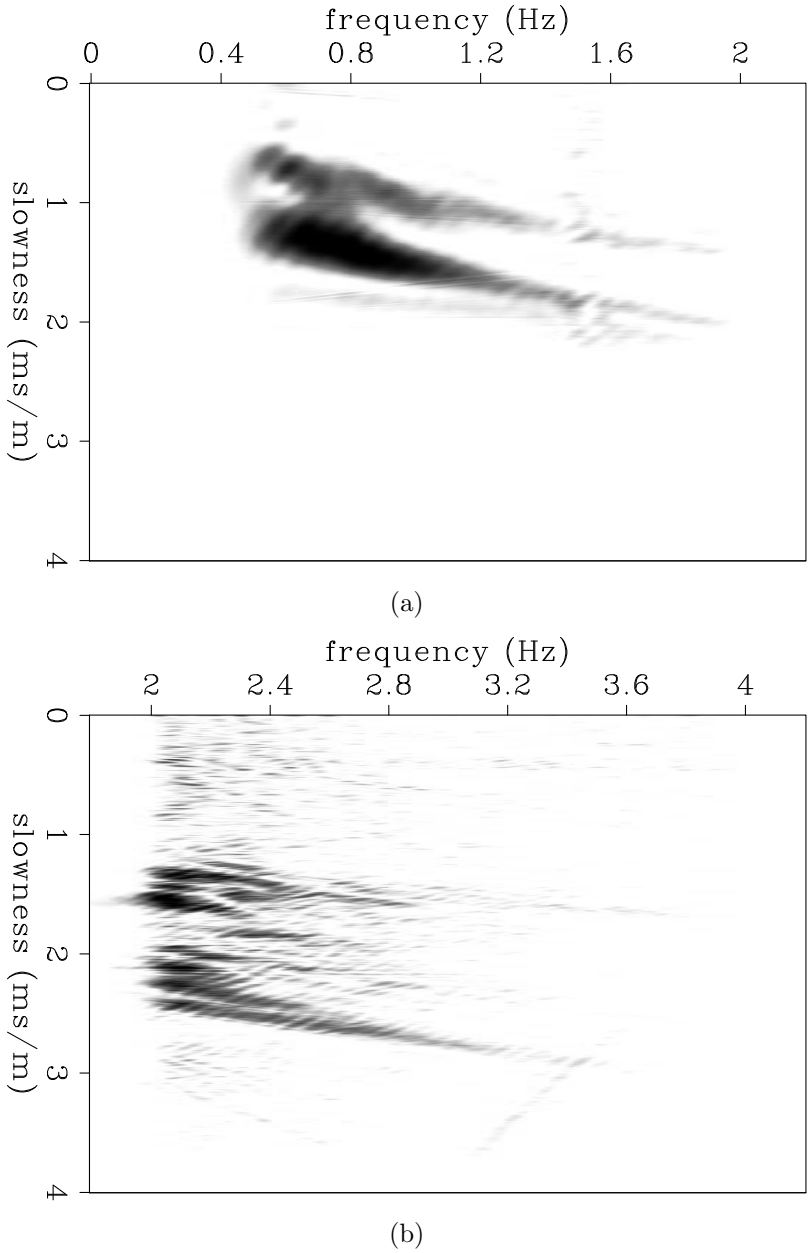

Figure 5: Dispersion images generated from the τ-p transformed gathers in Figure 4. Left: for frequencies between 0.5 and 2 Hz. Right: for frequencies between 2 and 4 Hz. [**CR**]

source gather for this frequency range due to the lack of convergence for the latter scenario. Much like the lower frequency range, there are the fundamental and first-order Rayleigh wave modes. At 2.2 Hz, there is a spectral peak near 2.2 ms/m, which corresponds to the fundamental mode travelling at 450 m/s, and a minor spectral peak near 1.5 ms/m, which corresponds to the first-order mode travelling at 660 m/s.

These observations fall in line with expectations for dispersive Rayleigh wave modes. Again, for a given wave mode, lower frequencies sense deeper and thus travel at higher velocities than at higher frequencies. Furthermore, the fundamental mode travels slower than the higher-order mode for the same frequency because higher-order modes typically sense deeper (Xia et al., 2003). Higher-order Rayleigh wave modes can potentially be used to help constrain shear wave velocities obtained from inverting dispersion curves.

SUMMARY AND FUTURE WORK

The goal of this report is to constrain the apparent velocity estimates for the Rayleigh and P-waves obtained from seismic interferometry. Chang et al. (2013) estimated the P-wave apparent velocity to be 2000 m/s, based on the slope of the stepout in the virtual super-source gather with 200 m offset binning. Here, I use a τ-p transform on the same super-source gather with 50 m offset binning to show that the velocity of the P-wave is closer to 2500 m/s. My dispersion analysis reveals two dispersive wave modes: the fundamental and the first-order Rayleigh wave modes. For a given frequency range, I find that the fundamental mode travels slower than the first-order mode.

The next step is to create phase velocity maps for different frequencies. From these maps, I can generate local dispersion curves that can be inverted for 1D shear velocity profiles. The presence of the first-order Rayleigh wave mode might help constrain those local dispersion curves and thus improve the shear velocity estimates. While I have estimated the velocity of the P-wave, I still need to determine whether this is a direct or a critically refracted P-wave. I therefore intend to stack more correlations into the super-source gather to improve the signal-to-noise ratio at shorter offsets.

ACKNOWLEDGMENTS

I gratefully acknowledge Signal Hill Petroleum, Inc. for access to this dataset and permission to publish. I also would like to thank Sjoerd de Ridder and Biondo Biondi for their guidance and support throughout this research.

REFERENCES

Bensen, G., M. Ritzwoller, M. Barmin, A. Levshin, F. Lin, M. Moschetti, N. Shapiro, and Y. Yang, 2007, Processing seismic ambient noise data to obtain reliable broad-

band surface wave dispersion measurements: Geophysical Journal International, **169**, 1239–1260.

Chang, J. P., S. de Ridder, and B. Biondi, 2013, Noise characterization and ambient noise cross-correlations at Long Beach: SEP-Report, **149**.

Claerbout, J., 1985, Imaging the Earth's Interior: Blackwell Science, Inc.

Stoffa, P., 1989, Tau-p: A Plane Wave Approach to the Analysis of Seismic Data: Kluwer Academic Publishers.

Wapenaar, K., D. Draganov, R. Snieder, X. Campman, and A. Verdel, 2010, Tutorial on seismic interferometry: Part 1–basic principles and applications: Geophysics, **75**, 75A195–75A209.

Xia, J., R. D. Miller, C. B. Park, and G. Tian, 2003, Inversion of high frequency surface waves with fundamental and higher modes: Journal of Applied Geophysics, **52**, 45–57.